Organic Geochemistry 195 (2024) 104830

Contents lists available at ScienceDirect

Organic Geochemistry

journal homepage: www.elsevier.com/locate/orggeochem

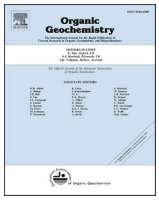

A paleoenvironmental and ecological analysis of biomarkers from the Eocene Fossil Basin, Green River Formation, U.S.A.

Amy L. Elson [a,*], Lorenz Schwark [a,b], Jessica H. Whiteside [c], Peter Hopper [a], Stephen F. Poropat [a], Alex I. Holman [a], Kliti Grice [a,*]

[a] Western Australian Organic and Isotope Geochemistry Centre, School of Earth and Planetary Sciences, The Institute for Geoscience Research, Curtin University, Australia
[b] Christian-Albrechts-University, Institute of Geosciences, Kiel, Germany
[c] San Diego State University, USA

ARTICLE INFO

Associate Editor — Josef P. Werne

Keywords:
Biomarkers
Exceptional fossil preservation
Green River Formation
Paleoenvironment
Fossil Basin
Eocene
Paleolake
EECO

ABSTRACT

Exceptionally well-preserved fossil specimens in the Fossil Basin of the Green River Formation (GRF) have made it the subject of extensive paleontological study, but the organic molecular framework that evolved during a key paleoclimatic and fossil-bearing interval during the early Eocene is poorly understood. Whereas the organic geochemistry of the larger co-eval GRF basins has been extensively characterized, our molecular understanding of the fossil-bearing layers in the Fossil Basin and the drivers of the exceptional fossilization therein remain unresolved. To bridge this gap, sediments from the famous 18″-layer — the fossiliferous horizon that is extensively quarried for exceptional soft-tissue fossils — were sampled for organic and isotopic geochemical characterisation. The results show that the Fossil Basin sedimentary archive is geochemically distinct from other GRF basins, as exemplified by the absence of the classical biomarker β-carotane and minimal evidence for the large green algal blooms that predominate in the other GRF lake basins. Photic zone euxinia (PZE), anoxia, and a freshwater cap enabled development of a productive and diverse ecosystem. Salinity and density stratification prevented vertical mixing of the water column and supported preservation of decaying carcasses. In contrast to other GRF basins, the small areal extent and ellipsoid shape of the Fossil Basin focussed terrestrial and freshwater inputs into the lake, resulting in ideal conditions for preservation of an exceptional fossil record.

1. Introduction

The "Fossil Basin" in the Eocene Green River Formation (GRF) represents one of the world's most exceptional lacustrine and fossil deposits. Despite representing the thinnest stratigraphic interval of the GRF (~11 m), the Fossil Butte Member (FBM) represents the greatest lateral expansion of the paleolake occupying Fossil Basin (Buchheim, 1994; Buchheim et al., 2015). The FBM is one of the world's most abundant and diverse fossil deposits, including numerous well-preserved fossilized fish and plants, along with reptiles, insects, and mammals (including early Cenozoic ancestors of bats and horses) (MacGinitie, 1969; Buchheim, 1994; Grande, 2013).

There has been debate around the drivers of exceptional preservation within the GRF (McGrew, 1975; Grande, 2001; Sullivan et al., 2012; Hellawell and Orr. 2012). Despite extensive research on these Eocene lakes, a holistic understanding of the paleoenvironment that resulted in the death and fossilisation of the organisms that lived in this lake has yet to be established. This paper utilizes biomarkers and their stable carbon isotopes from samples of the famous 18″ fossil layer, as well as elemental parameters indicative of redox conditions, water column stratification, terrigenous input, and PZE, to disentangle the drivers that enabled preservation of this remarkable lacustrine lagerstätte.

1.1. Geological context

The GRF was deposited in a network of continental interior lakes during the early–middle Eocene (~53.5–43 My; Sheliga, 1980; Remy, 1992; Smith et al., 2008; Fig. 1). The Fossil Basin is located within the Wyoming thrust belt and foreland basin area, and was deposited within a structurally controlled, wedge top basin. The first expression of the GRF in Fossil Basin is the fluvial–lacustrine overfilled facies (Bohacs et al., 2000) of the Hollow Road Member, with minimal fossil

* Corresponding authors.
E-mail address: Amy.Elson@curtin.edu.au (A.L. Elson).

https://doi.org/10.1016/j.orggeochem.2024.104830
Received 18 December 2023; Received in revised form 22 June 2024; Accepted 22 June 2024
Available online 27 June 2024
0146-6380/© 2024 The Author(s). Published by Elsevier Ltd. This is an open access article under the CC BY license (http://creativecommons.org/licenses/by/4.0/).

preservation. The lake depocenter had migrated to the north by the time of deposition of the FBM and the 18″ layer. The sampling location of this study represents a basin depocenter location during the 18″ layer (Buchheim et al., 2015; Figs. 1 and 2). The FBM is defined as a fluctuating–profundal facies and represents the deepest water deposit in the Fossil Basin, prior to the lake shallowing up during deposition of the evaporitic uppermost Angelo Member (Buchheim, 1994; Bohacs et al., 2000; Buchheim et al., 2011).

The most prolific fossil-bearing horizons within the FBM have been previously defined as a 'profundal kerogen-rich laminated micrite' (Buchheim and Eugster, 1998; Buchheim et al., 2011) and were deposited in the basin centre. Towards the shoreline, laminations thicken as calcium-rich fluvial waters mingled with the high alkalinity, bicarbonate-rich lacustrine water of the Fossil Basin paleolake, precipitating calcium carbonate (Buchheim and Eugster, 1998). The micrite is comprised of lighter (calcium carbonate-dominated) and darker (kerogen-dominated) laminae, with occasional siliciclastic and volcaniclastic material present. Improved geochronological dates from frequent ash layers of the Challis and Absaroka volcanic fields have permitted interbasin correlation of the various sedimentary expressions of the GRF (Smith et al., 2008, 2010; Buchheim et al., 2015), allowing for a deeper understanding of the Green River paleolake system in a broader paleoecological and climatic context.

1.2. Early Eocene

The early Eocene (~56–47.8 Ma) represents an interval of prolonged Cenozoic warmth that culminated in the Early Eocene Climatic Optimum (53.26–49.14 Ma; EECO), where atmospheric CO_2 concentrations reached ~1625 ± 760 parts per million by volume (Zachos et al., 2001, 2008; Jagniecki et al., 2013; Anagnostou et al., 2016; Lunt et al., 2017; Foster et al., 2017; Westerhold et al., 2018; Schaefer et al., 2022). Superimposed on this longer warming trend is a series of at least twenty probable greenhouse gas-induced periods of rapid warming where temperature spikes exceeded 5 °C, known commonly as hyperthermal events (Thomas et al., 2000; Cramer et al., 2003; Lourens et al., 2005; Zachos et al., 2008; Zeebe and Lourens, 2019). $\delta^{13}C_{organic}$ analysis of FBM contemporaneous floodplain and paleosol units from the Uinta Basin, GRF, identified negative shifts ($\delta^{13}C$ 2.5‰—5‰ VPDB) representing the early Eocene hyperthermal events expressed in the GRF (Gall et al., 2017; Birgenheier et al., 2019). Hyperthermal events argued to occur during eccentricity minima have also been identified in a $\delta^{13}C_{carbonate}$ and lacustrine lithologic record from the Greater Green River Basin of Wyoming (Smith et al., 2015); however, these events and their effects have not been constrained within the Fossil Basin.

During the coeval highstand and extension of Fossil Lake and Lake Gosiute, a hydrological connection formed between both lakes, to the south of Oyster Ridge (Fig. 2), which led to the deposition of the FBM in the Fossil Basin and the Tipton Member in the Greater Green River Basin (Buchheim et al., 2015).

1.3. Biomarker studies

Previous studies have identified several biomarkers in the GRF, including perhydro-β-carotane, various steranes and triterpanes and their aromatic counterparts, as well as gammacerane (Murphy et al., 1967; Collister et al., 1994; Koopmans et al., 1997). Previous work on the GRF have identified four dominant categories of lipid biomarkers:

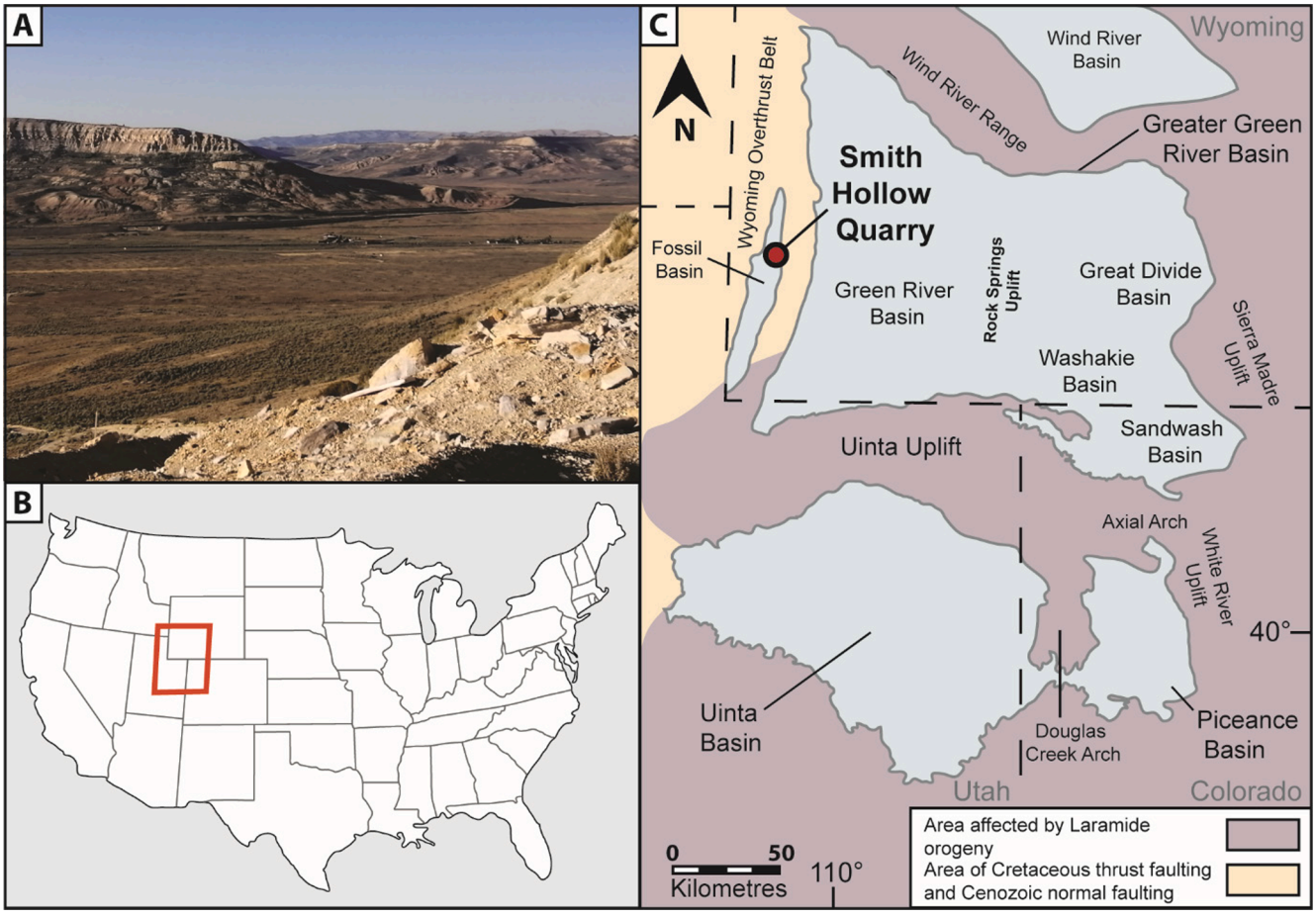

Fig. 1. (A) Overlook from Smith Hollow Quarry, Fossil Basin (B) Wyoming, Utah, and Colorado within the continental U.S.A. (C) GRF basins and the position of the field site, Smith Hollow Quarry and Fossil Basin, Wyoming.

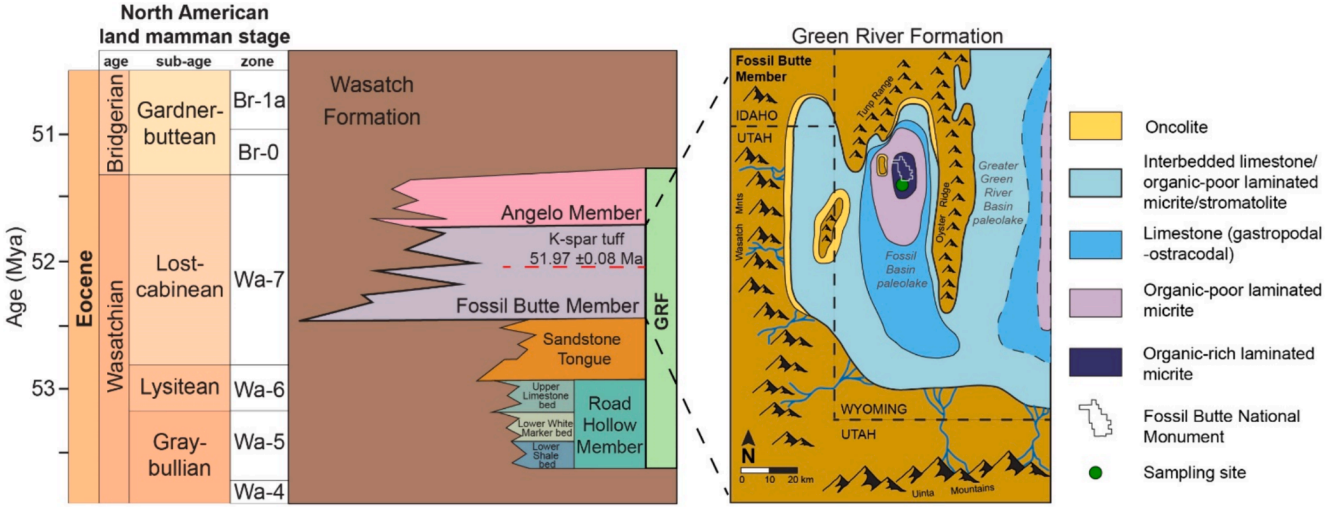

Fig. 2. Lithofacies map of the Fossil Butte Member, representing the lake highstand of Fossil Basin (Adapted from Buchheim et al., 2015).

terrestrial leaf wax-derived *n*-alkanes; hopanoids (bacterial); chlorophyll-derived isoprenoids; and algal-derived steranes (Tissot et al., 1978; Collister et al., 1994). Higher plants synthesize hydrocarbons with a strong predominance of odd-over-even numbered *n*-alkanes, which when preserved in the rock record can inform about terrigenous organic matter input. In particular, *n*-C_{27}, *n*-C_{29}, and *n*-C_{31} are indicative of vascular plant material, which when carried into local lacustrine basins is considered to be minimally transported by fluvial systems and to represent <2000 years of deposition (Davies-Vollum and Wing, 1998).

Regular isoprenoids, pristane (Pr), and phytane (Ph), are largely derived from the phytyl side chain of chlorophyll-*a*, the photoautotrophic pigment and precursor molecule involved in oxygenic photosynthesis during the light absorption and transfer into chemical energy (Eglinton et al., 1978). Ph, unlike Pr, is formed through the dehydroxylation of phytol, and an increased ratio of Pr: Ph has long been used as a general indicator of redox conditions (Didyk et al., 1978; ten Haven et al., 1987; Witkowski et al., 2018). Lower molecular weight *n*-alkanes (e.g., *n*-C_{17}) are frequently interpreted as being of aquatic origin, and comparison with terrestrially-derived material through various indices (i.e. average chain length, carbon preference index, terrestrial: aquatic ratio) can be a powerful tool for fingerprinting organic matter sources (Collister et al., 1994; Bourbonniere and Meyers, 1996; Ficken et al., 2000; Bi et al., 2005). The presence of gammacerane (derived from tetrahymanol, synthesised by bactiverous ciliates living at the chemocline) in large amounts suggests the presence of a stratified water column and potential hypersalinity in the depositional setting (Venkatesan, 1989; ten Haven et al., 1987; Sinninghe Damsté et al., 1995a,b; Grice et al., 1998c; Peters et al., 2004; Peters et al., 2005).

1.4. Exceptional fossilization

Drivers of exceptional fossilization, such as H_2S and bicarbonate released by sulfate reducing bacteria (SRB), and photic zone euxinia (PZE), have been identified in several sedimentary systems that host exceptionally preserved fossils (e.g., Devonian Gogo Formation; Jurassic Posidonia Shale [Melendez et al., 2013; Plet et al., 2017]). However, despite the wealth of paleontological research conducted in the Fossil Basin, the taphonomic mechanisms that operate within this system remain enigmatic. This is, in part, a consequence of the sparsity of biomarker data from key fossil layers in the GRF, which can be attributed to a traditional focus on the evaporitic and oil shale layers in other GRF basins (Roehler, 1993; Smith et al., 2008; Elson et al., 2022; Walters et al., 2023). Fossils have been permineralized with calcite-rich minerals in the pore space, introduced by Ca^{2+}-rich tributaries feeding the Fossil Basin. This fluvial activity leached largely limestone-formed mountains proximal to the lake (Buchheim et al., 2015). Subsequent carbonization (loss of volatiles) and compression resulted in the striking dark brown and black fossils observed in the FBM (Grande, 1984, 2001). This study utilizes organic and inorganic geochemical tools to elucidate the paleoecological, environmental, and diagenetic drivers that enabled such exceptional soft-tissue preservation.

2. Methods

Fieldwork was undertaken in the Fossil Basin during August 2022. Multiple sedimentary matrix samples from the 18″ layer were collected from Smith Hollow Quarry, a commercial GRF fossil quarry (Fig. 1), south of Fossil Butte National Monument. These samples were freshly exhumed and immediately wrapped in aluminium foil to protect against organic contamination and photo-oxidation. Two rock samples were taken from the carbonate limestone laminations that host exceptionally preserved fish fossils: GR-SHQ-18″-11 and GR-SHQ-18″-12.

Matrix samples were prepared at the Western Australian- Organic and Isotope Geochemistry Centre using a tungsten carbide scribe (tips sonicated three times for 15 min in 9:1 dichloromethane: methanol (DCM:MeOH)) by removing exactly those laminae at the fish fossil layer. The sample material was ground to a fine powder using a pre-annealed (500 °C for 7 h) ceramic mortar and pestle, and Soxhlet extracted in glass wool-composed, pre-extracted thimbles using a mixture of DCM: MeOH (9:1 *v/v*, 72 h). Thimbles were twice-annealed and Soxhlet extracted (twice, 24 h), and screened for any contamination using gas chromatography–mass spectrometry (GC–MS). A blank pre-extracted thimble was extracted alongside each Soxhlet extraction, and activated copper was added to the round bottom flasks for the duration of the Soxhlet extraction to remove elemental sulfur. Small scale column chromatography of the weighed total lipid extracts enabled separation into aliphatic, aromatic, and polar compounds (see Maslen et al., 2011).

2.1. Gas chromatography (GC)–mass spectrometry (MS) and multiple reaction monitoring (MRM)

GC–MS analysis and biomarker identification was performed using an Agilent 5977B Mass- Selective Detector (MSD) interfaced to an Agilent 7890B gas chromatograph (GC) equipped with an Agilent 7693 auto-sampler and a DB-1MS UI capillary column (60 m length, 0.25 mm I.D., 0.25 um film thickness) for saturate analysis, and an Agilent 5975B Mass- Selective Detector (MSD) interfaced to an Agilent 6890N gas

chromatograph (GC) equipped with a 7683B auto-sampler and a DB-5MS UI capillary column (60 m length, 0.25 mm I.D., 0.25 um film thickness) for aromatic analysis. The GC-oven was heated from 40 °C to 325 °C at 3 °C/min with initial and final hold times of 1 and 30 min, respectively.

GC-MRM analysis and biomarker identification was performed using an Agilent 8890 GC interfaced to an Agilent 7010C Triple Quadrupole equipped with an Agilent 7693A auto-sampler and a DB-5MS UI capillary column (60 m length, 0.25 mm I.D., 0.25 um film thickness (122-5562UI). The GC-oven was heated from 60 °C to 220 °C at 8/min, then to 320 °C at 2/min with initial and final hold times of 2 and 28 min, respectively (inlet temperature 300 °C, 1.5 mL min^{-1} He carrier gas flow). Ions monitored in saturate fractions: steranes ($M^{\bullet+} \rightarrow 217$); hopanes ($M^{\bullet+} \rightarrow 191$). Ions monitored in aromatic fractions: isorenieratane (544.5 → 134); aryl isoprenoids (134 → 119).

2.2. Gas chromatography–isotope ratio–mass spectrometry (GC–IR–MS)

The $\delta^{13}C$ signature of pH and molecular weight *n*-alkanes, was measured using a Thermo Delta V Advantage irMS, coupled to a Thermo Trace GC Ultra via a GC Isolink and Conflo IV. Ions measured for CO_2 on the irMS were m/z 44, 45 and 46. Values were corrected to the Vienna Pee Dee Belemnite carbon isotope scale using an in-house standard containing a mixture of *n*-alkanes (*n*-C_{11}, *n*-C_{13}, *n*-C_{14}, *n*-C_{17}, *n*-C_{18}, *n*-C_{19} and *n*-C_{25}; with a known isotopic composition (from −25.3 to −32.2‰). Samples were measured in triplicate with 1 μL injections, and standard deviations for $\delta^{13}C$ were < 0.5‰ (1σ).

2.3. X-ray diffraction (XRD)

XRD analysis for the composition of the crystalline mineral phases was undertaken with a Bruker D8A, Bragg-Brentano geometry X-ray Diffractometer, containing a copper X-ray source. Phase pattern identification was completed with Eva and Topaz software.

3. Results

3.1. Gas chromatography (GC)–mass spectrometry (MS) and multiple reaction monitoring (MRM)

3.1.1. Aliphatic fraction

Pr/Ph values are very low (0.19 and 0.20), along with low Pr/C_{17} (0.81) and high Ph/C_{18} (4.05), indicating a relative preference for phytane (Didyk et al., 1978; ten Haven et al., 1987). Several *n*-alkane ratios have been developed for characterizing the *n*-alkane distribution and organic matter sources of a sample, including the odd-over-even predominance (OEP), carbon preference index (CPI), average chain length (ACL), terrestrial: aquatic ratio (TAR), and the C_{29}/C_{17} ratio (Scalan and Smith, 1970; Marzi et al., 1993; Bourbonniere and Meyers, 1996; Ficken et al., 2000). The OEP for GR-SHQ-18″-11 and GR-SHQ-18″-12 (hereafter referred to as 18″-11 and 18″-12) is 2.31 and 2.91, and TAR values are 59.9 and 25.02. The *n*-alkane distribution ratios CPI and ACL demonstrate an average higher carbon number, and for 18″-11 and 18″-12 are 4.42 and 5.73 (CPI), and 28.18 and 27.71 (ACL), respectively. The ratio between C_{29} and C_{17} *n*-alkanes can indicate the predominance of organic matter sources between higher plants and algal derivatives, and is 41.8 and 17.30, for 18″-11 and 18″-12. A representative distribution of acyclic and cyclic aliphatic hydrocarbons is presented in Fig. 3.

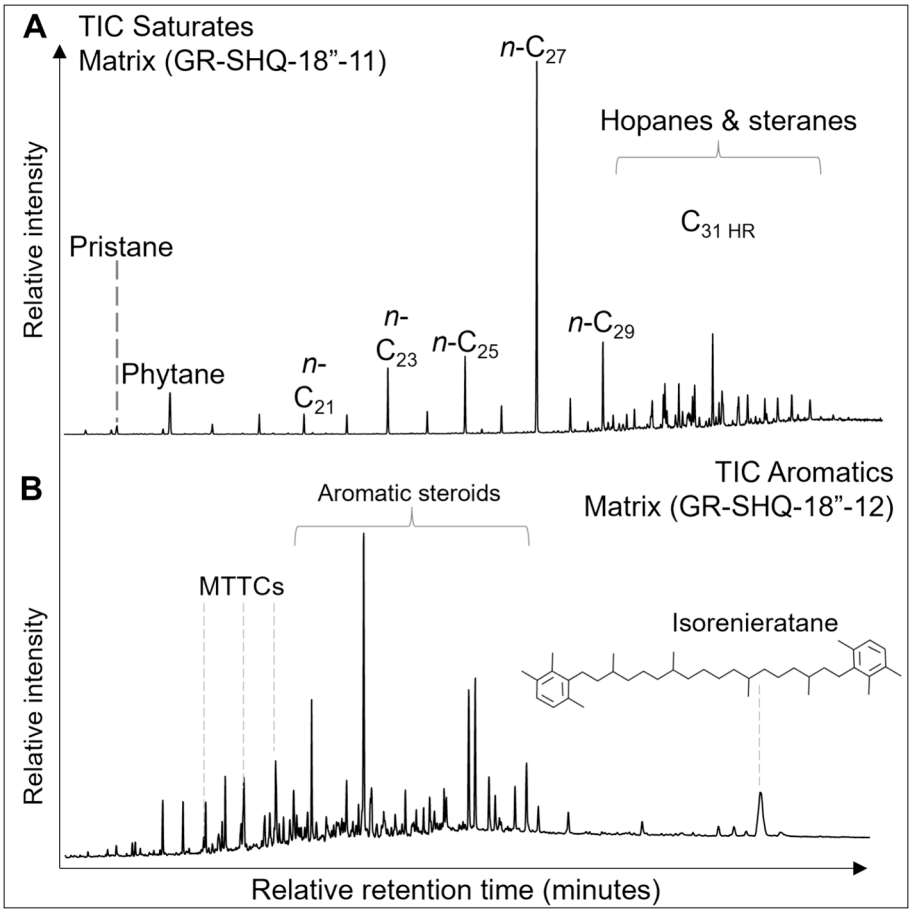

Fig. 3. (A) Total ion chromatogram (TIC) of the saturates fraction of GR-SHQ-18″-12. (B) TIC of the aromatic fraction of GR-SHQ-18″-12.

A suite of triterpenoid biomarkers is present in the 18″ layer samples, and common hopane occurrences and ratios are detailed hereafter. Notably, Ts/(Ts + Tm) values are identical in both samples (0.02), as are the βα/(βα + αβ) C_{30} hopane ratios (0.15). The gammacerane index (GI) is 0.28 and 0.31, in 18″-11 and 18″-12, and both samples contain extended hop(17,21)enes up to C_{35} (decreasing in abundance with increasing chain length).

The predictable thermodynamic behaviour between *S* (geologically favoured) and *R* (biologically favoured) epimers in C_{27}-C_{29} steranes and C_{31}-C_{35} hopanes allows inferences of the thermal maturity of samples (Köster et al., 1997). Low C_{29} 20*S*/20*R* sterane values are observed for both 18″-11 (0.11) and 18″-12 (0.12) matrixes. The total 20*S*/20*R* sterane and the C_{31} hopane 22*S*/(22*S* + 22*R*) values mirror this behavior for 18″-11 (0.20; 0.07) and 18″-12 (0.18 and 0.09). A high predominance of the 20*R* isomer for the $C_{27,28,29}$ ααα steranes in both samples is also noted.

C_{29} steranes constitute the majority of steranes preserved at 18″-11 (45.7 %) and 18″-12 (43.7 %), followed by C_{27} steranes (37.1 and 35.5 %, respectively). C_{28} steranes are still well represented (17.3 and 16.5 %, respectively) whereas C_{30} steranes contribute minimally (18.5 and 4.3 %) to the total sterane abundance. The hopane/sterane (total C_{27}-C_{30} hopanes/total C_{27}-C_{29} steranes) values for 18″-11 and 18″-12 are 3.62 and 2.71, and diasteranes are present in negligible amounts within the samples.

3.1.2. Aromatic fraction

A suite of methyl-, dimethyl-, and trimethyl methyltrimethyltridecylchromans (MTTCs) were identified at *m/z* 121; 135, and 149, respectively. This allowed for the calculation of the chroman ratio (5,7,8-trimethyl-MTTC/total MTTCs; Sinninghe Damsté et al., 1993; Tulipani et al., 2015) determined as 0.70 for 18″-11, and 0.56 for 18″-12. A dominant peak in the aromatic fraction is isorenieratane, found alongside a suite of carotenoid biomarkers including okenane, chlorobactane, β-isorenieratane, and renieratane identified *via* GC–MRM–MS comparison with carotenoid standards (Fig. 4). Also identified is perylene, a product of quinone pigments present in lignin-degrading fungi and formed from diagenetic processes (Jiang et al., 2000; Grice et al., 2009; Suzuki et al., 2010).

3.2. Compound specific carbon isotopes

Compound-specific $\delta^{13}C_{n\text{-alkane}}$ values from *n*-C_{23}–C_{31} are consistently depleted relative to $\delta^{13}C_{phytane}$. $\delta^{13}C_{phytane}$ values are −30.9‰ and −29.5‰ for 18″-11 and 18″-12. The mid-chain *n*-alkane isotope values (*n*-C_{23}, *n*-C_{25}; Table 1) are depleted relative to phytane and potentially reflect submerged or floating aquatic macrophytes. A potential contribution from limnic algae photosynthesizing in the paleolake might also contribute to the mid-chain *n*-alkanes $\delta^{13}C$ values (Cranwell, 1984) as they have also been shown to biosynthesize these (Cranwell, 1984; Robinson et al., 1989; Spaak et al., 2017; He et al., 2022), and consequently, isotope values might not preferentially derive from macrophytes but also from limnic algae.

$\delta^{13}C$ *n*-C_{23} values for both samples are –33.1‰ and –32.5‰, and $\delta^{13}C$ *n*-C_{25} values are –32.6‰ and –32.5‰. The longer chain *n*-alkanes (*n*-C_{27}, *n*-C_{29}, *n*-C_{31}) represent a leaf wax terrestrial contribution and might give insight into the local terrestrial carbon cycle. These values are similar for 18″-11 and 18″-12 for the *n*-C_{27} and *n*-C_{29} $\delta^{13}C$ measurements (*n*-C_{27}: –33.9‰ for both samples; *n*-C_{29}: −31.9‰ for both; *n*-C_{31}: –33.9‰ and −35.4‰), and are depleted relative to $\delta^{13}C_{phytane}$ (as seen in the mid-chain length *n*-alkanes).

3.3. XRD analysis

The major crystalline phase present is calcium carbonate ($CaCO_3$; 87.9%; 85.1%), along with a secondary component of ankerite (6.1%; 9.1%; an iron-rich magnesium carbonate), and minor amounts of dolomite (2.8%; 3.3%), and quartz (3.2%; 2.6%). Model uncertainty error was calculated from the Topaz analysis software (Table 2).

3.4. Rock-Eval

Rock-Eval analysis measured total organic content (TOC), S1, S2, and temperature of maximum pyrolysis yield (Tmax). Hydrogen index values are quite high, at 816 mgHC/gTOC and 750 mgHC/gTOC for 18″-11 and 18″-12, compared to reasonable oxygen index values of 21 $mgCO_2$/gTOC and 27 $mgCO_2$/gTOC, and TOC values of 4.9 and 2.46 wt %, respectively. Tmax for both samples is under the threshold for hydrocarbon generation (430 °C for 18″-11 and 419 °C for 18″-12). The volatile hydrocarbon content (S1; mgHC/g rock) is low for 18″-11 (0.15) and 18″-12 (0.14), and the remaining hydrocarbon generative potential

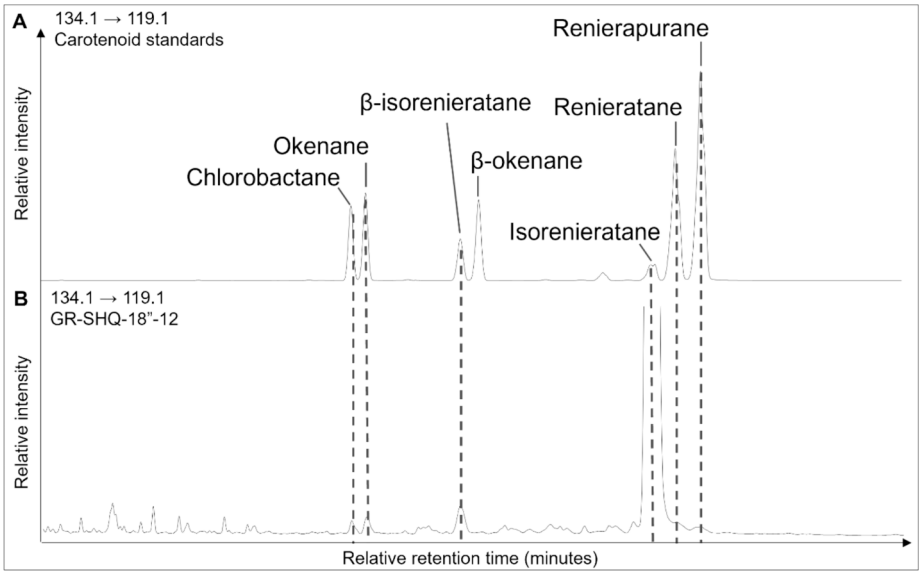

Fig. 4. MRM trace of the aromatic fraction monitored at 134.1 → 119.1, for (A) carotenoid standard and (B) GR-SHQ-18″-12. Comparison with the carotenoid standard with study samples allowed for identification of a suite of carotenoids, alongside a very prominent isorenieratane peak.

Table 1
Common biomarker and geochemical ratios reported for GR-SHQ-18″-11, and GR-SHQ-18″-12 matrix samples. Carbon isotope values represent the average of triplicate analysis.

	GR-SHQ-18″-12	GR-SHQ-18″-11
Pr/Ph	0.19	0.20
Gammacerane Index: (Gammacerane/$C_{30}\alpha\beta$ Hopane)	0.28	0.31
Chroman ratio: (5,7,8 trimethyl-MTTC/total MTTC's)	0.70	0.56
Ts/(Ts + Tm): (Ts = 17α-22, 29, 30-trinorhopane; Tm = 18a-22, 29, 20-trisnorneohopane)	0.02	0.02
20*S*/20*R* ratio for total C_{27} to C_{29} steranes	0.20	0.18
C_{29} steranes 20*S*/20*R*	0.11	0.12
C_{30} hopanes βα/(βα + αβ)	0.15	0.15
C_{31} hopanes 22*S*/(22*S* + 22*R*)	0.07	0.09
Odd-over-Even Predominance (OEP): (C_{27}+(6xC_{29}) + C_{31})/(4xC_{28}+(4xC_{30}))	2.31	2.91
Average Chain Length (ACL): ((25 × C_{25})+(27 × C_{27})+(29 × C_{29})+(31 × C_{31})+(33 × C_{33}))/(C_{25} + C_{27} + C_{29} + C_{31} + C_{33})	28.2	27.7
Carbon Preference Index (CPI): (2×(C_{23} + C_{25} + C_{27} + C_{29}))/(C_{22} + 2×(C_{24} + C_{26} + C_{28}) + C_{30})	4.42	5.73
Terrestrial: Aquatic Ratio (TAR): (C_{27} + C_{29} + C_{31})/(C_{15} + C_{17} + C_{19})	59.95	25.02
C_{29}/C_{17}	41.8	17.3
Hopanes/steranes	3.62	2.71
C_{27}:C_{28}:C_{29} steranes (%)	37: 17: 46	36: 17: 44
Compound specific carbon isotope analysis (‰; *n* = 3)		
Phytane	−30.9 (±0.19)	−29.5 (±0.39)
n- C_{23}alkane	−33.1 (±0.49)	−32.5 (±0.31)
n- C_{25}alkane	−32.6 (±0.13)	−32.5 (±0.11)
n- C_{27} alkane	−33.9 (±0.19)	−33.9 (±0.16)
n- C_{29} alkane	−31.9 (±0.14)	−31.9 (±0.18)
n C_{31}-alkane	−33.9 (±0.31)	−35.4 (±0.16)

Table 2
X-ray diffraction and Rock-Eval data for GR-SHQ-18″-11 and GR-SHQ-18″-12.

XRD analysis of crystalline phases present in matrix (%)	GR-SHQ-18″-11	GR-SHQ-18″-12
Calcium carbonate	87.9 (±4.6)	85.1 (±2.9)
Ankerite	6.1 (±0.3)	9.1 (±0.8)
Quartz	3.2 (±0.2)	2.6 (±0.1)
Dolomite	2.8 (±0.2)	3.3 (±0.2)
Rock-Eval data (triplicate analysis)		
TOC (wt.%)	4.9 (SD: 0.16)	2.45 (SD < 0.01)
T_{max} (°C)	430 (SD: 0)	419 (SD < 0.01)
S1 (mgHC/g rock)	0.15 (SD: 0)	0.16 (SD: 0.03)
S2 (mgHC/g rock)	40.3 (SD: 1.5)	18.5 (SD: 0.41)
Hydrogen Index (mgHC/gTOC)	816 (SD: 7)	754 (SD: 18)
Oxygen Index ($mgCO_2$/gTOC)	21 (SD: 3)	27 (SD: 1)

of the samples (S2; mgHC/g rock) much higher for both (40.3 and 18.44, correspondingly).

4. Discussion

4.1. Thermal maturity

Both samples share very similar hopane and sterane ratios that are considered indicators of thermal maturity (Table 1), suggesting conformable conditions during diagenesis in the 18″ layer. A high amount of the C_{27} 22, 29, 30-trisnor-17β-hopane coincident with very low Ts/Tm values indicate that the 18″ layer did not experience sufficient burial to generate any hydrocarbons. An abundance of extended hopenes also supports a relatively low thermal maturity and has been observed in a variety of hypersaline environments (Boon et al., 1983; ten Haven et al., 1985, 1988; Schwark et al., 1998; Jiang et al., 2018). Elevated values of the *R* (thermally unstable biological) over *S* (stable geological) epimer in the hopane and sterane ratios support an interpretation of low thermal maturities (Table 1), and a predominance of ααα 20*R* isomerization in the $C_{27,28,29}$ steranes is also congruent with this.

Interestingly, when observing the isomerization of extended hopenes, the S epimer is dominant over the *R* epimer, suggesting the hopene isomers have reached equilibrium during minor thermal maturation and/or sulfurization of the *R* epimer (Köster et al., 1997). The organic geochemistry maturity ratios are harmonious with Rock-Eval data (low T_{max} and S1 values; Table 2), which also indicate relatively low levels of thermal maturation during the diagenetic history of the fossil layers. Variations in values between the two samples may be due to different vertical positions within the 18″ layer.

These results from Fossil Basin are harmonious with organic geochemical studies of coeval basins from the GRF and suggest minimal thermal maturation for the FBM and coincident lakes of the GRF (Collister et al., 1992; Horsfield et al., 1994; Elson et al., 2022).

4.2. Sources of organic matter

Vascular plants synthesise hydrocarbons with a strong predominance of odd-over-even numbered *n*-alkanes, and long chain $C_{25\text{-}33}$ *n*-alkanes are indicative of leaf wax material transported in from the shallow shore and terrestrial realm (Scalan and Smith, 1970; Marzi et al., 1993; Bourbonniere and Meyers, 1996; Ficken et al., 2000). The *n*-alkane derived OEP, ACL, CPI, and TAR values all support an increased amount of terrigenous lipids (long chain *n*-alkanes) preserved over aquatic lipids (short chain *n*-alkanes; $<C_{20}$), likely transported from the surrounding highlands to the Fossil Basin paleolake. Leaf waxes are robust biomolecules that survive fluvial transport, and due to natural buoyancy, can float to the center of lakes before sinking (Davies-Vollum and Wing, 1998).

High predominance of the C_{25} *n*-alkane and long-chain *n*-alkanes, usually derived from terrestrial leaf waxes, has in some instances been reported to reflect aquatic macrophyte or freshwater algal input (Cranwell, 1984; He et al., 2022).

Aquatic macrophytes include vascular plants (rooted, floating, and emerging), macro-algae, liverworts, and mosses (Miller and White, 2007). Emergent macrophytes have been found to contain *n*-alkane distributions characteristic of terrestrial higher plants i.e., $>n\text{-}C_{27}$ (Cranwell, 1984; Feakins et al., 2007), however, the *n*-alkane distribution of submerged/ floating macrophytes maximize at $n\text{-}C_{25}$. Mid-chain *n*-alkane $\delta^{13}C$ values tentatively suggest a floating macrophyte or macroalgae source over rooted (Table 1; Chikaraishi et al., 2004b) and a lack of rooting structures preserved within basin center facies suggest that rooting/emergent macrophytes were not a large contributor to the *n*-alkane distribution in the samples (Grande, 1994). However, the large coastline-to-lake surface area ratio of the paleolake compared to the other basins (Fig. 1) could have allowed for a large contribution of aquatic macrophyte wax lipids transported *ex situ* to the basin center, and the abnormally elevated pCO_2 of the EECO may also have contributed to depleted $\delta^{13}C$ values. These additional factors highlight a need for caution when considering the sources of long-chained *n*-alkanes (Nichols et al., 1988; Volkman, 1988; Lichtfouse et al., 1994; Gong and Hollander, 1997; McKirdy et al., 2010; Summons et al., 2013; Lowe et al., 2022).

Rock-Eval data indicates an algal derived, Type I organic matter

character with high TOC values comparable to optimal source rock values. Intriguingly, two common biomarkers associated with GRF oil-shale facies — β-carotane and biomarkers of *Botryococcus braunii* (e.g., botryococcane, lycopane, macrocyclic alkanes; McKirdy et al., 1986; Grice et al., 1998a; Grice et al., 2001; Audino et al., 2001) — were not observed.

This suggests minor input from green algal blooms, unlike the prominent algal input observed in other GFR paleolakes (Moldowan and Seifert, 1980; Collister et al., 1992; Horsfield et al., 1994). Alternatively, dilution of TOC values by rapid carbonate precipitation, and higher plant wax input, might contribute to the differences observed between the Fossil Basin and other GRF basins. A higher predominance of plant wax preserved may be the result of lower thermal maturities preventing transformation of short-chain (C_{14}-C_{18}) algal lipids to corresponding *n*-alkanes, favoring higher molecular weight *n*-alkanes. A high leaf wax predominance coupled with the presence of a salinity stratification biomarker, gammacerane, may also indicate preferential decay of short chain hydrocarbons by halophilic bacterial heterotrophs (Al-Mailem et al., 2010). Cyanobacterial blooms might have existed in the place of green-algal blooms; however, a lack of high amounts of *n*-C_{17} and a moderate amount of mid-chained *n*-alkanes suggest cyanobacteria blooms might not have been not abundant in Fossil Basin. Moderate hopane: sterane ratio values suggest a mixed bacterial vs. algal input of organic matter.

Relatively low TOC values compared to other GRF basins (such as the Uinta and Piceance basins, exceeding 40 wt% TOC; Collister et al., 1992; Horsfield et al., 1994; Elson et al., 2022), are attributed to severe carbonate dilution. Organic productivity in the paleolake, though, might have been driven by a combination of high terrestrial nutrient input and photosynthetic primary productivity in the surface waters. This terrestrial input could have been episodic or potentially seasonally driven, during the high energy precipitation regime of the EECO in the region (Tulipani et al., 2014; Gall et al., 2017; Birgenheier et al., 2019).

A predominance of C_{29} steranes (Table 1), over C_{27} steranes and C_{28} steranes suggests that a major sterol contributor to the Fossil Basin paleolake derived from common sources of C_{29} sterols, which include higher plants, eustigmatophytes, chrysophytes, and green algae (Volkman, 2003). C_{27} steranes also comprise a lesser, but still very substantial component and are abundant in animals and red algae (Grice et al., 1998b; Peters et al., 2004; Peters et al., 2005). A high abundance of hopanoids alongside the presence of perylene suggests microbial and fungal organic matter degradation (Huang and Meinschein, 1979; Moldowan et al., 1985).

4.3. Distribution of stable isotopes

To evaluate the relationship of these exceptional fossil-bearing layers and primary productivity, paleolake productivity in Fossil Basin was reconstructed using the $\delta^{13}C$ of Ph. The $\delta^{13}C_{phytane}$ values, if proven to be derived from aquatic organic matter instead of terrestrial sources, represent an integrated $\delta^{13}C$ value of the whole chlorophyll-producing community in the lake. During intervals of increased primary productivity in lake environments, the growth rates of phytoplankton will be more rapid, resulting in a decreased carbon isotope fractionation rate (Pancost and Pagani, 2005; Witkowski et al., 2018). This may be a factor affecting isotope values in the Fossil Paleolake. Enriched $\delta^{13}C_{phytane}$, relative to $\delta^{13}C_{n\text{-alkane}}$ values in the 18″ layer could be indicative of a predominantly algal source of the phytane, and different biosynthetic pathways (Schouten et al., 1998; Grice et al., 2005). Such differences might have resulted in varying isotopic fractionation from different biosynthetic pathways, between the terrestrial-sourced higher plants, and photoautotrophs residing within the water column (Schouten et al., 1998). Submerged aquatic macrophytes can be slightly ^{13}C-enriched relative to long chain *n*-alkanes due to the utilization of isotopically heavy HCO_3^- in a highly alkaline lake system. However, *n*-C_{23} and *n*-C_{25} are depleted relative to *n*-C_{29} in the Fossil Basin paleolake, suggesting either these alkanes were, in part, produced by lacustrine algae, or that the bicarbonate equilibrium is perturbed by increased photosynthetic activity and biologically induced pH changes (Mook et al., 1974; Sharkey and Berry, 1985; Falkowski, 1991).

Carbon isotope values for the *n*-C_{27}, C_{29}, and C_{31} alkanes are slightly depleted w.r.t other GRF basins (Collister et al., 1994) in both of the sedimentary matrix sample indicating a slightly different plant source (s). The presence of isorenieratane, alongside a suite of other carotenoids (okenane, chlorobactane, β-isorenieratane, renieratane) in both 18″ layer matrix samples indicate bacterial sulfate reduction in the paleolake, and euxinic conditions within the photic zone. Leaf wax values are depleted in ^{13}C compared to *n*-C_{29} in the coeval GRF Piceance basin (−28.8 to −31.7‰, average of −29.9‰; Collister et al., 1994). This might suggest higher levels of primary productivity in the catchment area, or perhaps differing local conditions (Fig. 1).

4.4. Paleoenvironment

Pr/Ph is very low for both samples, indicating highly reducing conditions. These values may be perturbed by processes such as mass transport deposits and other sources of phytol (Didyk et al., 1978; ten Haven et al., 1987). However, other geochemical data support the redox assessment, such as a moderate GI, which indicates ciliates living at the chemocline and the presence of stratified water layers (Sinninghe Damsté et al., 1995a,b). Isorenieratane can be derived from the carotenoid pigment isorenieratene biosynthesised by *Chlorobi,* and is potential evidence for photic zone euxinia (PZE) conditions (Summons and Powell, 1986; Grice et al., 2005). Detailed MRM analysis (Fig. 4) showed the presence of okenane, chlorobactane and isorenieratane indicative of purple, green-green and green–brown sulfur bacteria, respectively. Although it has been observed that isorenieratane may also derive from cyanobacterial carotenoids (Graham and Bryant, 2008; Cui et al., 2020) or *β*-carotene (Koopmans et al., 1997), the presence of PZE- related carotenoids within the aromatic fraction of the sedimentary matrix samples, and evidence of an already anoxic and stratified water column (e.g. low Pr/Ph, gammacerane), support the likelihood of PZE conditions during the FBM. Furthermore, coarser grains (indicative of fluvial activity) are minimally present in the sediment mineralogy; most of the sedimentation originates from calcium carbonate precipitation induced from primary productivity (Table 1).

The lack of diasteranes and negligible values of clay from XRD data in both matrix samples suggest a minor input from clay-rich source rocks. XRD peaks are fully symmetric and gaussian in appearance, suggesting a relative lack of amorphous material. The absence of broad low intensity peaks, which when present indicate an amorphous component to the matrix, also supports this interpretation. Amorphous phases might be present; however, they are likely under the limit of detection (<1%; Vyverberg et al., 2018). The platelet nature of clay minerals results in ready identification in XRD analysis, and so these minerals are usually well represented in XRD spectra if present.

A co-occurrence of moderate GI values and *Chlorobi* biomarkers in both samples support the presence of a chemocline, whereby salinity stratification and PZE conditions prevailed (Murphy et al., 1967; Sinninghe Damsté et al., 1995b; Tulipani et al., 2015). The MTTC index is proposed to reflect conditions above the chemocline, and the ratio between different chroman isomers has been established as a proxy for paleosalinity or freshwater incursions (Sinninghe Damsté et al., 1993; Sinninghe Damsté and de Leeuw, 1995; Tulipani et al., 2015) depending on the chroman index and the relationship with Pr/Ph. The high chroman ratio, and low Pr/Ph values of these samples, suggest a productive freshwater cap was present on the Fossil Basin paleolake during deposition of the 18″ layer.

The relatively high MTTC index could be a result of increased fluvial and plant input transported into the lake during episodic high energy precipitation, driven by the humid and hothouse EECO (~53–49 Ma) climate regime (Gall et al., 2017; Birgenheier et al., 2019; Cramwinckel

et al., 2023). This could have resulted in the development of freshwater incursions during the FBM, providing an optimal habitat for the diverse flora and fauna in the catchment of the Fossil Basin (Zachos et al., 2008; Tulipani et al., 2014; Westerhold et al., 2018). An alternate formation of MTTCs is via early diagenetic condensation reactions forming these compounds from phytol, by cyclisation with higher plant-derived alkylphenols (Li et al., 1995; Tulipani et al., 2014; Barakat and Rullkötter, 1997). The correlation with Pr/Ph and other paleoecological indicators suggests a freshwater origin for the MTTCs, and the presence of lower salinity in the upper water column (Fig. 5; Schwark et al., 1998; Didyk et al., 1978; Tulipani et al., 2015), demonstrating the separate vertical positions of ecological niches for the organisms, on which the GI and the MTTC indices are based. Density variations from saline and freshwater input baffled vertical mixing of the water column and precipitated a sharp chemo- and halocline in the Fossil Basin paleolake (Sinninghe Damsté et al., 1993; Tulipani et al., 2015).

The presence of perylene is often viewed as an indicator of terrigenous input (Orr and Grady, 1967; Aizenshtat, 1973; Jiang et al., 2000; Guilick et al., 2019) however, it can be produced by other organisms, including crinoids and some insects (Grice et al., 2009; Suzuki et al., 2010). The lack of crinoids in the Fossil Basin paleontological record excludes this source, and insect fossils are more commonly associated with lake margin facies in the FBM, rather than the depocenter (Fig. 2; Grande, 1984,2001). Terrigenous nutrient input was likely intensified seasonally, with an influx of freshwater enhancing primary productivity, and concomitantly providing a source of cations for carbonate precipitation. The FBM and deposition of the 18″ layer is coincident with the early phases of the EECO (K Spar tuff is dated at ~51.97 Ma; EECO ~ 53–49 Ma; Smith et al., 2008, 2010; Zachos et al., 2008; Tulipani et al., 2015; Westerhold et al., 2018). The Uinta Basin of the GRF records thick ephemeral sandstone sheets during the early Eocene hyperthermals, driven by high energy precipitation. Sediments comprising these sandstone sections were transported as far south as Arizona, indicating well-developed and high energy ephemeral systems controlling sedimentation in neighbouring GRF basins (Gall et al., 2017; Birgenheier et al., 2019). Fossil Basin was surrounded by hinterlands of the Rocky, Wasatch, and Uinta Mountains, and so more protected from the large-scale fluvial systems that developed in the south. The lack of coarser grains at the 18″ layer, evident from XRD and visual analysis, support a low energy environment, and distal to larger-clast sources.

4.5. Implications for exceptional preservation in the GRF

Taphonomic experiments on fish have identified that the high pH (alkaline) and high salinity characteristics of the GRF were potential key factors in early fossilisation (Briggs and Wilby, 1996; Gäb et al., 2020; Gerschermann et al., 2021; Clements et al., 2022). While anoxia might be important to deterring scavenging, it does not prevent the onset of decomposition (Allison, 1988). When considering the preservation of fish, other crucial factors include: sufficiently high hydrostatic pressure within the water column to ensure sinking of the carcass; and a sufficiently deep water body to overcome the buoyancy of the swim bladder (Gäb et al., 2020). Cooler lake waters also promote the sinking of fish carcasses, by contrast with warmer waters that favour carcass bloating, which generally results in rapid decay (Allison, 1986; Gäb et al., 2020).

The FBM has an exceptionally high percentage of vertebrates fossilized as well-articulated specimens: 68% of 385 samples from the 18″ layer were identified as perfect samples in one study (McGrew, 1975), and another more recent study returned 70% perfect samples from 1133 fish fossils (Sullivan et al., 2012). This excellent fossilization is not replicated across other GRF lake basins. Consequently, multiple explanations have been proposed as the key drivers of fossilization in the Fossil Basin, including: storm-driven overturning of the water column; H_2S poisoning; microbial mats; and algal blooms (McGrew, 1975; Grande, 2001; Sullivan et al., 2012; Hellawell and Orr, 2012). Algal blooms and microbial mats are present in other GRF basins, although during deposition of the FBM, southern basins of the GRF had very high sedimentation rates that would have obstructed high primary productivity and filled accommodation space required for a thriving lacustrine ecosystem (Gall et al., 2017; Birgenheier et al., 2019).

High molecular weight *n*-alkanes, primarily sourced from leaf waxes shedding off terrestrial higher plants and transported into the Fossil Basin catchment area, are present in very high amounts. Although this is a feature coincident with other GRF lakes, terrigenous material within

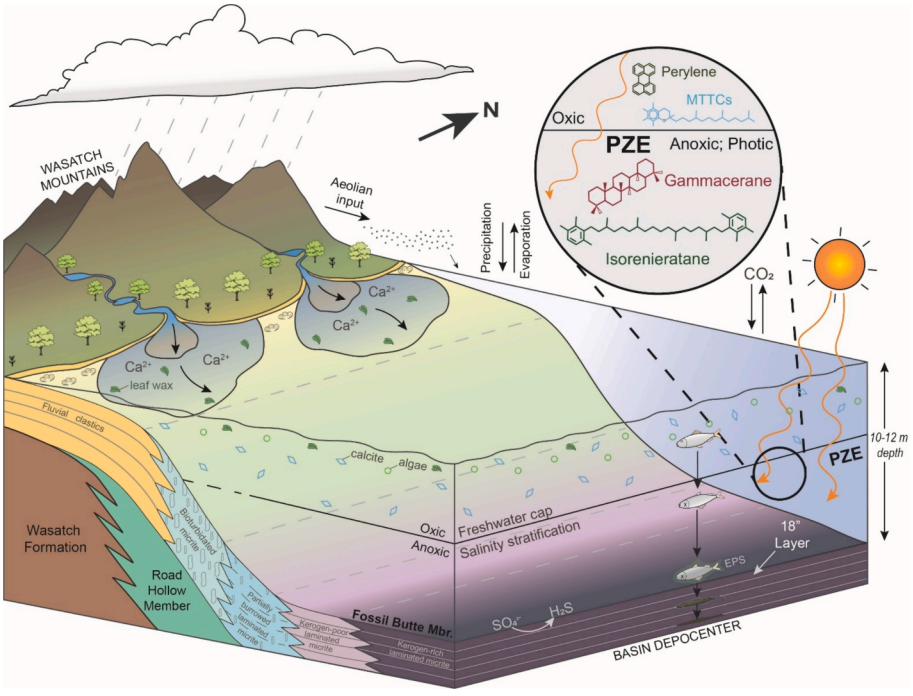

Fig. 5. Basin model of the Fossil Basin during deposition of the 18″ layer Lagerstätte in the Fossil Butte Member, and important paleoenvironmental markers identified in the 18″ layer samples (adapted from Tulipani et al., 2015; Buchheim et al., 2015; Elson, 2021).

the most distal confines of the lake basin is very high in the Fossil Basin (Collister et al., 1992; Elson et al., 2022).

A reason for this variance could be the different basin shape and small size compared to the other GRF basins (Fig. 1). The Fossil Basin paleolake contains the majority of the exceptional fossil specimens found, and was the smallest and the deepest of the three Green River paleolakes (Grande, 1984) with a maximum extent of 60 km by 30 km (Buchheim, 1994). The narrow ellipsoidal lake shape (i.e., a high shoreline development index; Hutchinson, 1957) could result in an overrepresentation of terrestrial material relative to the other GRF basins, with a larger surface area (resulting in an increase of *n*-alkane dilution over a larger basin area; >20 times the size of Fossil Basin). This might have increased the potential for a partial decoupling of biomarker proxies where plant material is incorporated, as excessive terrestrial material transported into the lake would dilute algal biomarker signals. An elliptical shape and high shoreline development index might have supported the development of littoral ecosystems and high biological productivity (Wetzel and Likens, 2000; Wetzel, 2001). The narrow lake shape, and greater lake depth of the Fossil Basin compared to the other GRF basins, would have supported development of stronger water column stratification (Valero-Garcés and Kelts, 1995) during the deposition of the 18″ layer. The morphometric properties of the Fossil Basin paleolake also resulted in cooler water column temperature — this is key to mitigating against the bloat-and-float, and promoting the sinking and burial, of carcasses (Gäb et al., 2020). This contrasts with the adjacent and much larger Greater Green River Basin, which is much topographically flatter and shallower in water depth. This resulted in weaker water column stratification and therefore higher scavenging and degradation of carcasses (Smith et al., 2008, 2010; Smith and Carroll, 2015; Buchheim et al., 2015).

Carbonate laminae are thought to result from calcite precipitation in response to episodic inflow of calcium-rich inflows, into the oversaturated bicarbonate and alkaline lake waters of Fossil Basin (Buchheim and Eugster, 1998). These laminations thin towards the basin center and were estimated at approximately 100 mm ka^{-1} for the main fish bearing units of the Fossil Basin paleolake (Grande, 1984; Smith et al., 2008), suggesting rapid carbonate precipitation and resultant burial of organic material. Carbonate precipitation is considered mostly chemical in origin (Eugster and Kelts, 1983) with the warmer EECO climate resulting in increased lake surface evaporation and concentration of bicarbonate material (Buchheim and Eugster, 1998; Zachos et al., 2001; Cramwinckel et al., 2023). During higher productivity in summer months, temperature-dependent photosynthetic activity of microbes and macrophytic plants in the upper water column caused precipitation of calcium carbonate in 'whiting' events (Kelts and Hsü, 1978; Schultze-Lam et al., 1997). It is likely that the Fossil Basin had multiple carbonate precipitation events annually, similar to other GRF basins (Elson et al., 2022), because of the reduced temperature gradients between seasons during the EECO (Lunt et al., 2020).

Tectonics and climate are critical controls of the distribution of carbonates in lake environments, primarily by driving: morphological change of the lake; input and output of ions through surface and ground water, wind, and rainfall processes; and the seasonality and temperature of the lake climate (Bohacs et al., 2000; Buchheim et al., 2015). The EECO climate and superimposed Eocene hyperthermal regime, driving an intensified hydrological cycle, might have led to increased terrestrial material and nutrient input to the lake, supporting stratification of freshwater and denser saline water and enhancing primary productivity (Zachos et al., 2001; Birgenheier et al., 2019; Cramwinckel et al., 2023). These conditions within a smaller, more isolated (from massive ephemeral sediment input; Gall et al., 2017) lacustrine basin might have created perfect conditions for fossil preservation, in stark contrast to other GRF basins. A freshwater cap developed within the smaller lake basin and enabled diverse and complex ecosystems to exist within the photic zone of the Fossil Basin paleolake, and stratification alongside anoxic and euxinic conditions inhibited rapid degradation of fossil specimens. The other GRF basins lacked the fossilization potential of Fossil Basin, as carcasses could not sink to a sufficient depth to be protected from scavenging, or high siliciclastic input clouded the water column and lowered primary productivity. This is not to say that diverse ecosystems did not exist in the neighboring Green River basins; it is simply more likely that their preservation potential might have been much lower compared to conditions in the Fossil Basin paleolake.

The eponymous fossil record of Fossil Basin sets it apart from other GRF basins. It is possible, even likely, that ecosystems across the entire region were complex and diverse; and yet, none of the other basins preserve them in such detail. The unique morphometric parameters of the Fossil Basin paleolake appear to have created a paleoenvironment that was periodically optimal for most organisms as a habitat during the warm and wet EECO climate (Zachos et al., 2001; Birgenheier et al., 2019; Cramwinckel et al., 2023). However, these parameters also enabled their carcasses to be rapidly buried (by high carbonate precipitation) and mineralized such that they were exceptionally preserved as fossils.

5. Conclusions

The Fossil Basin fossil record formed from the smallest and shortest-lived of the Green River paleolakes. It was deposited during the hot, humid conditions of the EECO, and contains a lacustrine lagerstätte unmatched in the other GRF basins. Exceptional preservation within Fossil Basin has made it a focus of paleontological research, but a paucity of organic geochemical studies has resulted in uncertainty over the geochemical conditions that enabled the generation of its diverse ecosystem and the exceptional preservation of soft tissue-containing fossils.

This study shows the Fossil Basin paleolake was geochemically distinct from other GRF paleolakes, lacking the large algal blooms that characterize the oil-shale deposition in paleolakes Uinta and Gosiute. MTTCs, Pr/Ph, gammacerane, and isorenieratane biomarkers all indicate the development of a salinity and density-driven stratification of the Fossil Lake at the 18″ layer. Anoxia and PZE were present at this interval, inhibiting degradation of fossil soft tissues. Additionally, a freshwater cap developed at the surface of the lake, which likely enabled habitat space for diverse and complex ecosystems within the paleolake of the Fossil Basin. The morphometric properties of the Fossil Basin paleolake, i.e., a deep, narrow basin with a high shoreline index, distinguish it from the other Green River basins. The above properties and processes may have simultaneously enhanced the nutrient supply and freshwater ecological space, which allowed for a complex ecosystem to develop alongside conditions that promoted robust stratification, high carbonate precipitation, and potentially lethal PZE. These factors ensured optimal conditions for burial and fossilization.

The Fossil Basin of the Green River Formation is well suited for further detailed geochemical studies. The present study provides a framework for future research directed at a more complete reconstruction of the ecological, paleoenvironmental, and diagenetic history of the Fossil Basin during deposition of the FBM.

CRediT authorship contribution statement

Amy L. Elson: Writing – original draft, Methodology, Investigation, Formal analysis, Data curation. **Lorenz Schwark:** Writing – review & editing. **Jessica H. Whiteside:** Writing – review & editing, Data curation. **Peter Hopper:** Writing – review & editing. **Stephen F. Poropat:** Writing – review & editing. **Alex I. Holman:** Writing – review & editing. **Kliti Grice:** Writing – review & editing, Supervision, Resources, Methodology, Funding acquisition, Formal analysis, Conceptualization.

Declaration of competing interest

The authors declare the following financial interests/personal

relationships which may be considered as potential competing interests: Amy Elson reports financial support was provided by Australian Research Council. If there are other authors, they declare that they have no known competing financial interests or personal relationships that could have appeared to influence the work reported in this paper.

Data availability

Data will be made available on request.

Acknowledgements

This research was funded by the Australian Research Council (ARC), for an ARC-Laureate Fellowship grant (FL210100103) awarded to Prof. Kliti Grice. Fieldwork was undertaken by ALE and JHW (funded by the Laureate Fellowship grant). We would like to thank Mr. Todd Hoeg as the owner of Smith Hollow Quarry, for allowing us access, and Fossil Butte Monument staff member Dr. Arvid Aase, for direction and support. We thank the support from the John de Laeter Centre for XRD analysis, and technical support from Kate Putman, as well as to Prof. Phillipe Schaeffer for providing carotenoid standards for comparison in GC-MRM-MS analyses. We would also like to thank The Institute of Geoscience Research (TIGeR) for supporting the research and fossilization project. We would also like to thank ChemCentre and Valerie Brown for support with initial MRM analysis, and particularly the editors and reviewers for feedback and comments that improved the manuscript.

References

Aizenshtat, Z., 1973. Perylene and its geochemical significance. Geochimica et Cosmochimica Acta 37 (3), 559–567.
Allison, P.A., 1986. Soft-bodied animals in the fossil record: The role of decay in fragmentation during transport. Geology 14, 979–981.
Allison, P.A., 1988. The role of anoxia in the decay and mineralization of proteinaceous macro-fossils. Paleobiology 14, 139–154.
Al-Mailem, D.M., Sorkhoh, N.A., Al-Awadhi, H., Eliyas, M., Radwan, S.S., 2010. Biodegradation of crude oil and pure hydrocarbons by extreme halophilic archaea from hypersaline coasts of the Arabian Gulf. Extremophiles 14, 321–328.
Anagnostou, E., John, E.H., Edgar, K.M., Foster, G.L., Ridgwell, A., Inglis, G.N., Pancost, R.D., Lunt, D.J., Pearson, P.N., 2016. Changing atmospheric CO_2 concentration was the primary driver of early Cenozoic climate. Nature 533 (7603), 380–384.
Audino, M., Grice, K., Alexander, R., Boreham, C.J., Kagi, R.I., 2001. Unusual distribution of monomethylalkanes in Botryococcus braunii–rich samples: origin and significance. Geochimica et Cosmochimica Acta 65 (12), 1995–2006.
Barakat, A.O., Rullkötter, J., 1997. A comparative study of molecular paleosalinity indicators: chromans, tocopherols and C_{20} isoprenoid thiophenes in Miocene lake sediments (Nördlinger Ries, Southern Germany). Aquatic Geochemistry 3, 169–190.
Bi, X., Sheng, G., Liu, X., Li, C. Fu, J., 2005. Molecular and carbon and hydrogen isotopic composition of n-alkanes in plant leaf waxes. Organic Geochemistry, 36(10), 1405-1417.
Birgenheier, L.P., Vanden Berg, M.D., Plink-Björklund, P., Gall, R.D., Rosencrans, E., Rosenberg, M.J., Toms, L.C., Morris, J., 2019. Climate impact on fluvial-lake system evolution, Eocene Green River Formation, Uinta Basin, Utah, USA. Geological Society of America Bulletin. 132, 562–587.
Bohacs, K.M., Carroll, A.R., Neal, J.E., Mankiewicz, P.J., 2000. Lake-basin type, source potential, and hydrocarbon character: an integrated sequence-stratigraphic–geochemical framework. In: Gierlowski-Kordesch, E.H., Kelts, K.R. (Eds.), Lake Basins through Space and Time, American Association of Petroleum Geologists, Vol. 46. https://doi.org/10.1306/St46706C1.
Boon, J.J., Hines, H., Burlingame, A.L., Klok, J., Rijpstra, W.I.C., Leeuw, J.W.de, Edmunds, K.E., Eglinton, G., 1983. Organic geochemical studies of Solar Lake laminated cyanobacterial mats. In: Bjorøy M., et al. (Eds.), Advances in Organic Geochemistry 1981, Wiley, Chichester (1983), pp. 207-227.
Bourbonniere, R.A., Meyers, P.A., 1996. Sedimentary geolipid records of historical changes in the watersheds and productivities of Lakes Ontario and Erie. Limnology and Oceanography 41, 352–359. https://doi.org/10.4319/lo.1996.41.2.0352.
Briggs, D., Wilby, P., 1996. The role of the calcium carbonate-calcium switch in the mineralization of soft-bodied fossils. Journal of the Geological Society, London 153, 665–668.
Buchheim, H.P., 1994. Paleoenvironments, lithofacies and varves of the Fossil Butte Member of the Eocene Green River Formation, southwestern Wyoming. Rocky Mountain Geology 30 (1), 3–14.
Buchheim, H.P., Cushman, R.A., Biaggi, R.E., 2011. Stratigraphic revision of the Green River Formation in Fossil Basin, Wyoming. Rocky Mountain Geology 46 (2), 165–181.
Buchheim, H.P., Biaggi, R.E., Cushman, R.A., 2015. Stratigraphy and interbasinal correlations between Fossil and the Green River Basin, Wyoming. In: Smith, M.E., Carroll, A.R. (Eds.), Stratigraphy and Paleolimnology of the Green River Formation. Western USA, pp. 127–151.
Buchheim, H.P., Eugster, H.P., 1998. Eocene Fossil Lake: The Green River Formation of Fossil Basin, southwestern Wyoming. In: Pitman, J.K., Carroll, A.R. (Eds.), Modern and ancient lake systems new problems and perspectives, pp. 191–208.
Chikaraishi, Y., Naraoka, H., Poulson, S.R., 2004. Hydrogen and carbon isotopic fractionations of lipid biosynthesis among terrestrial (C3, C4 and CAM) and aquatic plants. Phytochemistry 65 (10), 1369–1381.
Clements, T., Purnell, M.A., Gabbott, S., 2022. Experimental analysis of organ decay and pH gradients within a carcass and the implications for phosphatization of soft tissues. Palaeontology 65, 1–13. https://doi.org/10.1111/pala.12617.
Collister, J.W., Summons, R.E., Lichtfouse, E., Hayes, J.M., 1992. An isotopic biogeochemical study of the Green River oil shale. Organic Geochemistry 19, 265–276.
Collister, J.W., Lichtfouse, E., Hieshima, G., Hayes, J.M., 1994. Partial resolution of sources of *n*-alkanes in the saline portion of the Parachute Creek Member, Green River Formation (Piceance Creek Basin, Colorado). Organic Geochemistry 21, 645–659.
Cramer, B.S., Wright, J.D., Kent, D.V., Aubry, M.P., 2003. Orbital climate forcing of $\delta^{13}C$ excursions in the late Paleocene–early Eocene (chrons C24n–C25n). Paleoceanography 18 (4), 1–25. https://doi.org/10.1029/2003PA000909.
Cramwinckel, M.J., Burls, N.J., Fahad, A.A., Knapp, S., West, C.K., Reichgelt, T., Greenwood, D.R., Chan, W.L., Donnadieu, Y., Hutchinson, D.K., de Boer, A.M., 2023. Global and zonal-mean hydrological response to early Eocene warmth. Paleoceanography and Paleoclimatology, e2022PA004542.
Cranwell, P.A., 1984. Alkyl esters, mid chain ketones and fatty acids in late glacial and postglacial lacustrine sediments. Organic Geochemistry 6, 115–124.
Cui, X., Liu, X.L., Shen, G., Ma, J., Husain, F., Rocher, D., Zumberge, J.E., Bryant, D.A., Summons, R.E., 2020. Niche expansion for phototrophic sulfur bacteria at the Proterozoic-Phanerozoic transition. Proceedings of the National Academy of Sciences 117 (30), 17599–17606.
Davies-Vollum, K.S., Wing, S.L., 1998. Sedimentological, taphonomic, and climatic aspects of Eocene swamp deposits (Willwood Formation, Bighorn Basin, Wyoming). Palaios 13 (1), 28–40.
Didyk, B.M., Simoneit, B.R.T., Brassell, S.T., Eglinton, G., 1978. Organic geochemical indicators of palaeoenvironmental conditions of sedimentation. Nature 272, 216–222.
Eglinton, G., Brassell, S.C., Simoneit, B.R.T., Didyk, B.M., 1978. Organic geochemical indicators of palaeoenvironmental conditions of sedimentation. Nature 272 (5650), 216–222.
Elson, A.L., Rohrssen, M., Marshall, J., Inglis, G.N., Whiteside, J.H., 2022. Hydroclimate variability in the United States continental interior during the early Eocene Climatic Optimum. Palaeogeography, Palaeoclimatology, Palaeoecology 595, 110959.
Elson, A.L., 2021. Descent from the hyperthermals: persistent organic-matter rich lakes in the Eocene, Doctoral dissertation, University of Southampton, 175p.
Eugster, H.P., Kelts, K., 1983. Lacustrine chemical lakes and sediments. In: Goudie, A., Pye, K. (Eds.), Chemical Sediments and Geomorphology. Academic Press, New York, N.Y., pp. 321–368
Falkowski, P.G., 1991. Species variability in the fractionation of ^{13}C and ^{12}C by marine phytoplankton. Journal of Plankton Research 13, 21–28.
Feakins, S.J., Eglinton, T.I., Demenocal, P.B., 2007. A comparison of biomarker records of northeast African vegetation from lacustrine and marine sediments (ca. 3.40 Ma). Organic Geochemistry 38 (10), 1607–1624.
Ficken, K.J., Li, B., Swain, D., Eglinton, G., 2000. An n-alkane proxy for the sedimentary input of submerged/floating freshwater aquatic macrophytes. Organic Geochemistry 31, 745–749.
Foster, G.L., Royer, D.L., Lunt, D.J., 2017. Future climate forcing potentially without precedent in the last 420 million years. Nature Communications 8, 14845.
Gäb, F., Ballhaus, C., Stinnesbeck, E., Kral, A.G., Janssen, K., Bierbaum, G., 2020. Experimental taphonomy of fish-role of elevated pressure, salinity and pH. Scientific Reports 10 (1), 7839.
Gall, R.D., Birgenheier, L.P., Vanden Berg, M.D., 2017. Highly seasonal and perennial fluvial facies: Implications for climate control on the Douglas Creek and Parachute Creek members, Green River Formation, Southeastern Uinta Basin, Utah, U.S.A. Journal of Sedimentary Research 87 (9), 1019–1047. https://doi.org/10.2110/jsr.2017.54.
Gerschermann, S., Ballhaus, C., Gäb, F., 2021. Rheological properties of calcite oozes: implications for the fossilisation in the plattenkalks of the Solnhofen-Eichstätt lagoons in the Franconian Alb, Germany. Plos One 16 (6), e0252469.
Gong, C., Hollander, D.J., 1997. Differential contribution of bacteria to sedimentary organic matter in oxic and anoxic environments, Santa Monica Basin, California. Organic Geochemistry 26, 545–563. https://doi.org/10.1016/S0146-6380(97)00018-1.
Graham, J.E., Bryant, D.A., 2008. The biosynthetic pathway for synechoxanthin, an aromatic carotenoid synthesized by the euryhaline, unicellular cyanobacterium Synechococcus sp. strain PCC 7002. Journal of Bacteriology 190, 7966–7974.
Grande, L., 1984. Paleontology of the Green River Formation, with a review of the fish fauna. Bulletin of the Geological Survey of Wyoming 64, 333.
Grande, L., 1994. Studies of paleoenvironments and historical biogeography in the Fossil Butte and Laney Members of the Green River Formation. Rocky Mountain Geology 30 (1), 15–32.
Grande, L., 2001. An Updated Review of the Fish Faunas From the Green River Formation, the World's Most Productive Freshwater Lagerstätten. In: Gunnell, G.F.

(Ed.), Eocene Biodiversity. Topics in Geobiology. Springer, Boston, MA. https://doi.org/10.1007/978-1-4615-1271-4_1.
Grande, L., 2013. The lost world of fossil lake: snapshots from deep time. University of Chicago Press.
Grice, K., Schouten, S., Nissenbaum, A., Charrach, J., Damsté, J.S.S., 1998a. A remarkable paradox: sulfurised freshwater algal (Botryococcus braunii) lipids in an ancient hypersaline euxinic ecosystem. Organic Geochemistry 28 (3-4), 195–216.
Grice, K., Schouten, S., Peters, K.E., Damsté, J.S.S., 1998b. Molecular isotopic characterisation of hydrocarbon biomarkers in Palaeocene-Eocene evaporitic, lacustrine source rocks from the Jianghan Basin. China. Organic Geochemistry 29 (5-7), 1745–1764.
Grice, K., Klein Breteler, W.C.M., Schouten, S., Grossi, V., de Leeuw, J.W., Damsté, J.S.S., 1998c. Effects of zooplankton herbivory on biomarker proxy records. Paleoceanography 13, 686–693.
Grice, K., Audino, M., Boreham, C.J., Alexander, R., Kagi, R.I., 2001. Distributions and stable carbon isotopic compositions of biomarkers in torbanites from different palaeogeographical locations. Organic Geochemistry 32 (10), 1195–1210.
Grice, K., Cao, C., Love, G.D., Böttcher, M.E., Twitchett, R.J., Grosjean, E., Summons, R. E., Turgeon, S.C., Dunning, W., Jin, Y., 2005. Photic zone euxinia during the Permian-Triassic superanoxic event. Science 307 (5710), 706–709.
Grice, K., Lu, H., Atahan, P., Asif, M., Hallmann, C., Greenwood, P., Maslen, E., Tulipani, S., Williford, K., Dodson, J., 2009. New insights into the origin of perylene in geological samples. Geochimica et Cosmochimica Acta 73 (21), 6531–6543.
He, J., Jia, J., Guo, W., Jia, G., 2022. Archaeal tetraether lipids and their biphytane carbon isotope composition in sediments along an estuarine biogeochemical gradient. Geochimica et Cosmochimica Acta 318, 452–467.
Hellawell, J., Orr, P.J., 2012. Deciphering taphonomic processes in the Eocene Green River formation of Wyoming. Palaeobiodiversity and Palaeoenvironments 92, 353–365.
Horsfield, B., Curry, D.J., Bohacs, K., Littke, R., Rullkötter, J., Schenk, H.J., Radke, M., Schaefer, R.G., Carroll, A.R., Isaksen, G., Witte, E.G., 1994. Organic geochemistry of freshwater and alkaline lacustrine sediments in the Green River Formation of the Washakie Basin, Wyoming, USA. Organic Geochemistry 22 (3-5), 415–440.
Huang, W.Y., Meinschein, W.G., 1979. Sterols as ecological indicators. Geochimica et Cosmochimica Acta 43 (5), 739–745.
Hutchinson, G.E., 1957. A Treatise on Limnology: Volume 1. Geography, Physics and Chemistry. John Wiley and Sons, p. 1015.
Jagniecki, E.A., Jenkins, D.M., Lowenstein, T.K., Carroll, A.R., 2013. Experimental study of shortite ($Na_2Ca_2(CO_3)_3$) formation and application to the burial history of the Wilkins Peak Member, Green River Basin, Wyoming, USA. Geochimica et Cosmochimica Acta 115, 31–45.
Jiang, C., Alexander, R., Kagi, R.I., Murray, A.P., 2000. Origin of perylene in ancient sediments and its geological significance. Organic Geochemistry 31 (12), 1545–1559.
Jiang, H., Huang, J., Yang, J., 2018. Halotolerant and halophilic microbes and their environmental implications in saline and hypersaline lakes in Qinghai Province, China. Extremophiles in Eurasian Ecosystems: Ecology, Diversity, and Applications 299–316.
Kelts, K., Hsü, K.J., 1978. Freshwater carbonate sedimentation. In: Lerman, A. (Ed.), Lakes: Chemistry, Geology, Physics. Springer, New York, New York, NY, pp. 295–323.
Koopmans, M.P., De Leeuw, J.W., Damsté, J.S.S., 1997. Novel cyclised and aromatised diagenetic products of β-carotene in the Green River Shale. Organic Geochemistry 26 (7-8), 451–466.
Köster, J., Van Kaam-Peters, H.M., Koopmans, M.P., De Leeuw, J.W., Damsté, J.S.S., 1997. Sulphurisation of homohopanoids: Effects on carbon number distribution, speciation, and 22S22R epimer ratios. Geochimica et Cosmochimica Acta 61 (12), 2431–2452.
Li, M., Larter, S.R., Taylor, P., Jones, D.M., Bowler, B., Bjorøy, M., 1995. Biomarkers or not biomarkers? A new hypothesis for the origin of pristane involving derivation from methyltrimethyltridecylchromans (MTTCs) formed during diagenesis from chlorophyll and alkylphenols. Organic Geochemistry 23 (2), 159–167.
Lichtfouse, E., Derenne, S., Mariotti, A., Largeau, C., 1994. Possible algal origin of long chain odd n-alkanes in immature sediments as revealed by distributions and carbon isotope ratios. Organic Geochemistry 22, 1023–1027. https://doi.org/10.1016/0146-6380(94)90035-3.
Lourens, L.J., Sluijs, A., Kroon, D., Zachos, J.C., Thomas, E., Röhl, U., Bowles, J., Raffi, I., 2005. Astronomical pacing of late Palaeocene to early Eocene global warming events. Nature 435 (7045), 1083–1087.
Lowe, A.J., Diefendorf, A.F., Schlanser, K.M., Super, J., West, C.K., Greenwood, D.R., 2022. Dynamics of deposition and fossil preservation at the early Eocene Okanagan Highlands of British Columbia, Canada: insights from organic geochemistry. PALAIOS 37 (5), 185–200.
Lunt, D.J., Huber, M., Anagnostou, E., Baatsen, M.L., Caballero, R., DeConto, R., Dijkstra, H.A., Donnadieu, Y., Evans, D., Feng, R., Foster, G.L., 2017. The DeepMIP contribution to PMIP4: Experimental design for model simulations of the EECO, PETM, and pre-PETM (version 1.0). Geoscientific Model Development 10 (2), 889–901.
Lunt, D.J., Bragg, F., Chan, W.L., Hutchinson, D.K., Ladant, J.B., Niezgodzki, I., Steinig, S., Zhang, Z., Zhu, J., Abe-Ouchi, A., de Boer, A.M., 2020. DeepMIP: Model intercomparison of early Eocene climatic optimum (EECO) large-scale climate features and comparison with proxy data. Climate of the Past Discussions 2020, 1–27.
MacGinitie, H.D., 1969. The Eocene green River flora of northwestern Colorado and northeastern Utah. University of California Publications in Geological Sciences 83, 203.
Marzi, R., Torkelson, B.E., Olson, R.K., 1993. A revised carbon preference index. Organic Geochemistry 20 (8), 1303–1306.
Maslen, E., Grice, K., Le Métayer, P., Dawson, D., Edwards, D., 2011. Stable carbon isotopic compositions of individual aromatic hydrocarbons as source and age indicators in oils from western Australian basins. Organic Geochemistry 42 (4), 387–398.
McGrew, P.O., 1975. Taphonomy of Eocene fish from Fossil Basin, Wyoming. Fieldiana, Geology, Vol.33, No.14, Chicago : Field Museum of Natural History.
McKirdy, D.M., Cox, R.E., Volkman, J.K., Howell, V.J., 1986. Botryococcane in a new class of Australian non-marine crude oils. Nature 320 (6057), 57–59.
McKirdy, D., Krull, E., Mee, A., Haynes, D., Thorpe, C., Webster, L., Grice, K., Gell, P., 2010. Natural and cultural eutrophication in the Coorong, South Australia. Organic Geochemistry 41, 96–110.
Melendez, I., Grice, K. Schwark, L., 2013. Exceptional preservation of Palaeozoic steroids in a diagenetic continuum. Scientific reports, 3(1), 2768.
Miller, M.F., White, D.S., 2007. Ecological and evolutionary controls on the composition of marine and lake ichnofacies. In: Trace Fossils. Elsevier, pp. 531–544.
Moldowan, J.M., Seifert, W.K., 1980. First discovery of botryococcane in petroleum. Journal of the Chemical Society, Chemical Communications 19, 912–914.
Moldowan, J.M., Seifert, W.K., Gallegos, E.J., 1985. Relationship between petroleum composition and depositional environment of petroleum source rocks. AAPG Bulletin 69 (8), 1255–1268.
Mook, W.G., Bommerson, J.C., Staverman, W.H., 1974. Carbon isotope fractionation between dissolved bicarbonate and gaseous carbon dioxide. Earth and Planetary Science Letters 22 (2), 169–176.
Murphy, M.T., McCormick, A., Eglinton, G., 1967. Perhydro-β-carotene in the Green River shale. Science 157 (3792), 1040–1042.
Nichols, P.D., Palmisano, A.C., Volkman, J.K., Smith, G.A., White, D.C., 1988. Occurrence of an isoprenoid C25 diunsaturated alkene and high neutral lipid content in Antarctic sea ice diatom. Journal of Phycology 24, 90–96. https://doi.org/10.1111/j.1529-8817.1988.tb04459.x.
Orr, W.L., Grady, J.R., 1967. Perylene in basin sediments off southern California. Geochimica et Cosmochimica Acta 31 (7), 1201–1209.
Pancost, R.D., Pagani, M., 2005. Controls on the carbon isotopic compositions of lipids in marine environments. In: Volkman, J.K. (Ed.), Marine Organic Matter: Biomarkers, Isotopes and DNA, pp. 209–249.
Peters, K.E., Walters, C.C., Moldowan, J.M., 2004, *The Biomarker Guide, Vol. 1*. 2nd ed. Cambridge University Press.
Peters, K.E., Walters, C.C., Moldowan, J.M., 2005. Volume 2: Biomarkers and Isotopes in Petroleum Exploration and Earth History. The Biomarker Guide. Cambridge University Press, Cambridge, UK.
Plet, C., Grice, K., Pagès, A., Verrall, M., Coolen, M.J., Ruebsam, W., Rickard, W.D., Schwark, L., 2017. Palaeobiology of red and white blood cell-like structures, collagen and cholesterol in an ichthyosaur bone. Scientific Reports 7 (1), 13776.
Remy, R.R., 1992. Stratigraphy of the Eocene part of the Green River Formation in the south-central part of the Uinta Basin, Utah. No. 1787-BB.
Roehler, H.W., 1993. Eocene climates, depositional environments, and geography, greater Green River Basin, Wyoming, Utah, and Colorado. U.S. Geological Survey Professional Paper, 1506-F.
Robinson, N., Eglinton, G., Cranwell, P.A., Zeng, Y.B., 1989. Messel oil shale (western Germany): assessment of depositional palaeoenvironment from the content of biological marker compounds. Chemical Geology 76 (1–2), 153–173.
Scalan, E.S., Smith, J.E., 1970. An improved measure of the odd-even predominance in the normal alkanes of sediment extracts and petroleum. Geochimica et Cosmochimica Acta 34 (5), 611–620. https://doi.org/10.1016/0016-7037(70)90019-0.
Schaefer, B., Schwark, L., Böttcher, M.E., Smith, V., Coolen, M.J., Grice, K., 2022. Paleoenvironmental evolution during the Early Eocene Climate Optimum in the Chicxulub impact crater. Earth and Planetary Science Letters 589, 117589.
Schouten, S., Breteler, W.C.K., Blokker, P., Schogt, N., Rijpstra, W.I.C., Grice, K., Baas, M., Damsté, J.S.S., 1998. Biosynthetic effects on the stable carbon isotopic compositions of algal lipids: Implications for deciphering the carbon isotopic biomarker record. Geochimica et Cosmochimica Acta 62 (8), 1397–1406.
Schultze-Lam, S., Schultze-Lam, S., Beveridge, T.J., Des Marais, D.J., 1997. Whiting events: biogenic origin due to the photosynthetic activity of cyanobacterial picoplankton. Limnology and Oceanography 42 (1), 133–141.
Schwark, L., Vliex, M., Schaeffer, P., 1998. Geochemical characterization of Malm Zeta laminated carbonates from the Franconian Alb, SW-Germany (II). Organic Geochemistry 29 (8), 1921–1952.
Sharkey, T.D., Berry, J.A., 1985. Carbon isotope fractionation of algae as influenced by an inducible CO_2 concentrating mechanism. In: Lucas, W.J., Berry, J. (Eds.), Inorganic Carbon Uptake by Aquatic Photosynthetic Organisms, American Society of Plant Physiologists, pp. 389–401.
Sheliga, C.M., 1980. Sedimentology of the Eocene Green River Formation in Sevier and Sanpete Counties, Central Utah, Doctoral thesis. The Ohio State University.
Sinninghe Damsté, J.S., De Leeuw, J.W., 1995. Comments on 'Biomarkers or not Biomarkers. A new hypothesis for the origin of pristane involving derivation from methyltrimethyltridecylchromans (MTTCS) formed during diagenesis from chlorophyll and alkylphenols. Organic Geochemistry 23 (11/12), 1085–1087.
Sinninghe Damsté, J.S., de Leeuw, J.W., Wakeham, S.G., Hayes, J.M., Kohnen, M.E., 1993. Chemocline of the Black Sea. Nature 366 (6454), 416.
Sinninghe Damsté, J.S., Hoefs, M.J.L., de Leeuw, J.W., 1995a. In: Grimalt, J.O., Dorronsoro, C. (Eds.), Organic Geochemistry: Developments and Applications to Energy, Climate, Environment and Human History, pp. 158-161.

Sinninghe Damsté, J.S., Kenig, F., Koopmans, M.P., Köster, J., Schouten, S., Hayes, J.M., de Leeuw, J.W., 1995b. Evidence for gammacerane as an indicator of water column stratification. Geochimica et Cosmochimica Acta 59 (9), 1895–1900.
Smith, M.E., Carroll, A.R., 2015. Introduction to the Green River Formation. In: Smith, M.E., Carroll, A.R. (Eds.), Stratigraphy and Paleolimnology of the Green River Formation, Western USA. Springer, Dordrecht, pp. 1–12.
Smith, M.E., Carroll, A.R., Singer, B.S., 2008. Synoptic reconstruction of a major ancient lake system: Eocene Green River Formation, western United States. Geological Society of America Bulletin 120, 54–84. https://doi.org/10.1130/B26073.1.
Smith, M.E., Chamberlain, K.R., Singer, B.S., Carroll, A.R., 2010. Eocene clocks agree: Coeval $^{40}Ar/^{39}Ar$, U-Pb, and astronomical ages from the Green River Formation. Geology 38 (6), 527530.
Spaak, G., Edwards, D.S., Foster, C.B., Pages, A., Summons, R.E., Sherwood, N., Grice, K., 2017. Environmental conditions and microbial community structure during the Great Ordovician Biodiversification Event; a multi-disciplinary study from the Canning Basin, Western Australia. Global and Planetary Change 159, 93–112.
Sullivan, S.P., Grande, L., Gau, A., McAllister, C.S., 2012. Taphonomy in North America's Most Productive Freshwater Fossil Locality: Fossil Basin, Wyoming. Fieldiana Life and Earth Sciences 2012 (5), 1–4.
Summons, R.E., Powell, T.G., 1986. Chlorobiaceae in Palaeozoic seas revealed by biological markers, isotopes and geology. Nature 319 (6056), 763–765.
Summons, R.E., Bird, L.R., Gillespie, A.L., Pruss, S.B., Roberts, M., Sessions, A.L., 2013. Lipid biomarkers in ooids from different locations and ages: evidence for a common bacterial flora. Geobiology 11, 420–436. https://doi.org/10.1111/gbi.12047.
Suzuki, N., Yessalina, S., Kikuchi, T., 2010. Probable fungal origin of perylene in Late Cretaceous to Paleogene terrestrial sedimentary rocks of northeastern Japan as indicated from stable carbon isotopes. Organic Geochemistry 41 (3), 234–241.
ten Haven, H.L., De Leeuw, J.W., Schenck, P.A., 1985. Organic geochemical studies of a Messinian evaporitic basin, northern Apennines (Italy) I: Hydrocarbon biological markers for a hypersaline environment. Geochimica et Cosmochimica Acta 49 (10), 2181–2191.
ten Haven, H.L., de Leeuw, J.W., Rullkötter, J., Sinninghe Damsté, J.S., 1987. Restricted utility of the pristane/phytane ratio as a palaeoenvironmental indicator. Nature 330, 641–643.
ten Haven, H.L., De Leeuw, J.W., Sinninghe Damsté, J.S., Schenck, P.A., Palmer, S.E., Zumberge, J.E., 1988. Application of biological markers in the recognition of palaeohypersaline environments. Geological Society, London, Special Publications 40 (1), 123–130.
Thomas, E., Zachos, J.C., Bralower, T.J., 2000. Deep-sea environments on a warm earth: latest Paleocene-early Eocene. In: Huber, B.T, MacLeod, K.G., Wing, S.L. (Eds.), Warm Climates in Earth History. Cambridge University Press, Cambridge, UK, pp. 132–160.
Tissot, B., Deroo, G., Hood, A., 1978. Geochemical study of the Uinta Basin: Formation of petroleum from the Green River Formation. Geochimica et Cosmochimica Acta 42, 1469–1485.
Tulipani, S., Grice, K., Krull, E., Greenwood, P., Revill, A.T., 2014. Salinity variations in the northern Coorong Lagoon, South Australia: Significant changes in the ecosystem following human alteration to the natural water regime. Organic Geochemistry 75, 74–86.
Tulipani, S., Grice, K., Greenwood, P.F., Schwark, L., Böttcher, M.E., Summons, R.E., Foster, C.B., 2015. Molecular proxies as indicators of freshwater incursion-driven salinity stratification. Chemical Geology 409, 61–68.
Valero-Garcés, B.L., Kelts, K.R., 1995. A sedimentary facies model for perennial and meromictic saline lakes: Holocene Medicine Lake Basin, South Dakota, USA. Journal of Paleolimnology 14, 123–149.
Venkatesan, M.I., 1989. Tetrahymanol: its widespread occurrence and geochemical significance. Geochimica et Cosmochimica Acta 53 (11), 3095–3101.
Volkman, J.K., 1988. Biological marker compounds as indicators of the depositional environments of petroleum source rocks. Geological Society of London Special Publications 40, 103–122. https://doi.org/10.1144/GSL. SP. 1988.040.01.10.
Volkman, J.K., 2003. Sterols in microorganisms. Applied Microbiology & Biotechnology 60, 495–506.
Vyverberg, K.L., Jaeger, J.M., Dutton, A., 2018. Quantifying detection limits and uncertainty in X-ray diffraction mineralogical assessments of biogenic carbonates. Journal of Sedimentary Research 88 (11), 1261–1275.
Walters, A.P., Tierney, J.E., Zhu, J., Meyers, S.R., Graves, K., Carroll, A.R., 2023. Climate system asymmetries drive eccentricity pacing of hydroclimate during the early Eocene greenhouse. Science Advances 9 (31), eadg8022.
Westerhold, T., Röhl, U., Donner, B., Zachos, J.C., 2018. Global Extent of Early Eocene Hyperthermal Events: A new Pacific benthic foraminiferal isotope record from Shatsky Rise (ODP Site 1209). Paleoceanography and Paleoclimatology 33, 626–642. https://doi.org/10.1029/2017PA003306.
Wetzel, R.G., 2001. Limnology: lake and river ecosystems. Gulf Professional Publishing.
Wetzel, R.G., Likens, G., 2000. Limnological analyses. Springer Science and Business Media.
Witkowski, C.R., Weijers, J.W., Blais, B., Schouten, S., Sinninghe Damsté, J.S., 2018. Molecular fossils from phytoplankton reveal secular pCO_2 trend over the Phanerozoic. Science Advances 4 (11), eaat4556.
Zachos, J.C., Dickens, G.R., Zeebe, R.E., 2008. An early Cenozoic perspective on greenhouse warming and carbon-cycle dynamics. Nature 451, 279–283.
Zachos, J., Pagani, M., Sloan, L., Thomas, E., Billups, K., 2001. Trends, rhythms, and aberrations in global climate 65 Ma to present. Science 292, 686–693. https://doi.org/10.1126/science.1059412.
Zeebe, R.E., Lourens, L.J., 2019. Solar System chaos and the Paleocene-Eocene boundary age constrained by geology and astronomy. Science 365 (6456), 926–929.